2020 IEEE International Conference on Robotics and Automation (ICRA)
31 May - 31 August, 2020. Paris, France

Aerial Regrasping: Pivoting with Transformable Multilink Aerial Robot

Fan Shi[1], Moju Zhao[1], Masaki Murooka[1], Kei Okada[1], Masayuki Inaba[1]

***Abstract*— Regrasping is one of the most common and important manipulation skills used in our daily life. However, aerial regrasping has not been seriously investigated yet, since most of the aerial manipulator lacks dexterous manipulation abilities except for the basic pick-and-place. In this paper, we focus on pivoting a long box, which is one of the most classical problems among regrasping researches, using a transformable multilink aerial robot. First, we improve our previous controller by compensating for the external wrench. Second, we optimize the joints configuration of our transformable multilink drone for stable grasping form under the constraints of thrust force and joints effort. Third, we sequentially optimize the grasping force in the pivoting process. The optimization goal is to generate continous grasping force whilst maximizing the friction force in case of the downwash, which would influence the grasped object and is difficult to model. Fourth, we develop the impedance controller in joint space and admittance controller in task space. As far as we know, it is the first research to achieve extrinsic contact-aware regrasping task on aerial robots.**

I. Introduction

A. Motivation

With the development of aerial robots, interaction with the physical environment becomes a popular research field. Aerial manipulation is one of the most practical [1]. In most researches, drone is attached with a light gripper underneath the robot base to achieve an agile pick-and-place task [2], or even directly with a cable suspended to the small payload [3]. For large objects, researchers attach dual-arm manipulator [4] or team up several drone to transport cooperatively [5]–[7]

Recently, there is a new type of drone which could transform its shape during flying [8]–[12]. It could implement several manipulation tasks, such as whole-body grasping [9]–[11] with its body link. The advantage is to reduce extra weight and downwash effect because the attached extra manipulator arm is no longer required.

Comparing the previous aerial robot researches to manipulation community, aerial robots could already achieve accurate pick-and-place [2], [4], [9]–[11] and even peg-in-hole task [13]–[15].

However, for more dexterous manipulation skills such as regrasping [16]–[24], aerial robots have not been fully investigated yet. Regrasping actually is very common in human's daily life, such as re-orienting an in-hand smartphone to put it into pocket, or pivoting a heavy box from the ground. In industries especially factories and construction, regrasping is very important as well in changing the orientation of different components actively for further assembling process.

[1] F. Shi, M. Zhao, M. Murooka, K. Okada and M. Inaba are with Department of Creative-Infomatics, The University of Tokyo, 7-3-1 Hongo, Bunkyo-ku, Tokyo 113-8656, Japan shifan@jsk.t.u-tokyo.ac.jp

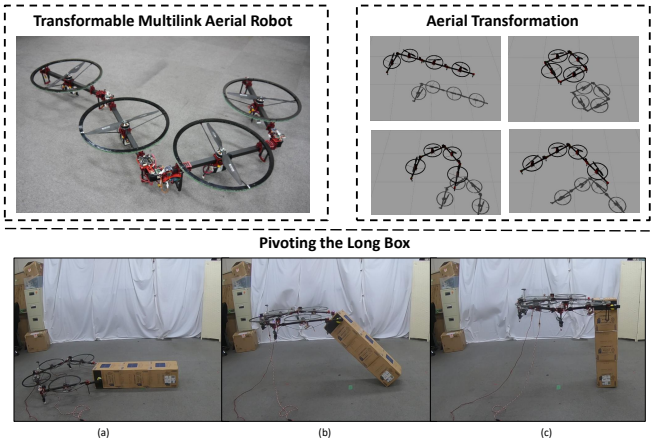

Fig. 1. The pivoting task is demonstrated with an aerial transformable multilink robot named HYDRUS (**H**orizontall**Y** **D**eformable aerial **R**obot with two-dimensional m**U**ltilink**S**). Experiment video: **https://fanshi14.github.io/me/icra20.html**

In manipulation community, regrasping has been thoroughly investigated among robot hand [16]–[18], manipulator arm [19]–[22] and humanoid robot [23], [24]. The robot could conduct in-hand object rotating, dual-arm components assembling, and even heavy bookshelf pivoting to achieve the dexterous interaction with physical environment.

In this paper, we introduce a novel aerial pivoting method to lift up a long box. The extrinsic dexterity [20] is utilized by keeping the end of box in contact with ground. Except for the accomplishment of re-orientation target, other advantages of aerial pivoting, comparing to simple gripping, lie in it saving almost half of strength and causing less center-of-mass (CoM) shift with the help of ground support. Robot would be more stable during the pivoting.

B. Related Work

Aerial Regrasping: Aerial regrasping firstly appears in our previous work to present an active dynamic regrasping [25]. The HYDRUS robot throws and re-catches a long box in the simulation to achieve re-orientation target. However, it requires extremely aggressive performance with large acceleration, which is too difficult and dangerous to implement on the physical robot. For other literature, since aerial regrasping is still a challenging task, the only related research we could find is lifting up a bar with manipulator attached hexarotor [26] . Because the bar is customized with a passive rotation joint on the end side, pivoting problem is simplified as an flight control problem with estimated external disturbance.

978-1-7281-7395-5/20/$31.00 ©2020 IEEE

The mechanics and constraints in general pivoting problem are not discussed.

Optimal Configuration of Transformable Drone: Since transformable drone is a novel field, most of the previous researches focus on flight controller and have not optimized the maneuvering configuration in [10]–[12]. The singular form of transformable drone is analyzed by [9] with geometry constraints. One of the most intuitive singularity cases is robot losing controllability when all the rotor is aligned in a straight line. [27] develops efficient motion primitive approach to optimize the joints trajectory avoiding unfeasible configuration during an agile table tennis task. In these work, the optimized configuration for transformable drone in interaction task is still in lack of investigation.

Interaction Control of Aerial Robot: The interaction control of drone starts from reacting to unexpected collision as [28]–[31] and quadrotor interaction with human in [26], [32] or cooperation with other drone in [6], [7]. The external wrench is estimated with basic onboard sensors, and admittance controller is developed in these researches to response in the passive way. For active interaction tasks such as peg-in-hole and valve turning, the impedance controller is developed in [12], [13], [33], [34]. The compliant force control is achieved in these researches.

Pivoting Planning through Contact: There are three main strategies in pivoting tasks, including utilizing gravity [35], inertia force [36] and extrinsic contact [17], [22]–[24]. Since aerial robot has limited agility and payload comparing to manipulator arm, utilizing extrinsic contact is the best approach. [17] designs two fingers to pivot a box on the table, and simplifies the problem by requiring contact points and object CoM are in the same line. [22] improves the approach without co-linear constraints and pivots a screw with parallel gripper. [23], [24] focus on task planner to pivot the heavy cabinet to a target position.

C. Contribution

The contribution of this paper is threefold:

(i). we develop the configuration optimization for transformable aerial robot in interaction tasks by optimizing rotor thrust force and joints effort under contact constraints.

(ii). we develop the force planner for aerial pivoting task to generate continous grasping force and diminish the influence of downwash.

(iii). we develop the impedance controller on joint space and admittance controller on task space, and succeed in pivoting a long box with HYDRUS robot.

To our best knowledge, it is the first research to achieve extrinsic contact-aware regrasping with aerial robots.

II. Problem Formulation

A. Transformable Aerial Robot

In this paper, we utilize HYDRUS, a two-dimensional transformable aerial robot developed in our previous research [9]. We attach an end effector on both head and tail link, equipped with 6-axis force/torque (FT) sensor and a sphere soft gripper with large friction coefficient.

B. Pivoting Task

Pivoting could be regarded as a primitive strategy in regrasping community. The target of pivoting task in this paper is to re-orient a long box from lying on the ground to being perpendicular against the ground.

Based on the pivoting analysis in Sec. I-B, our approach is to utilize extrinsic contact to lift up the long box. As Fig. 1, the end of the box would keep in contact with ground and the front would be grasped by the end effectors of our robot.

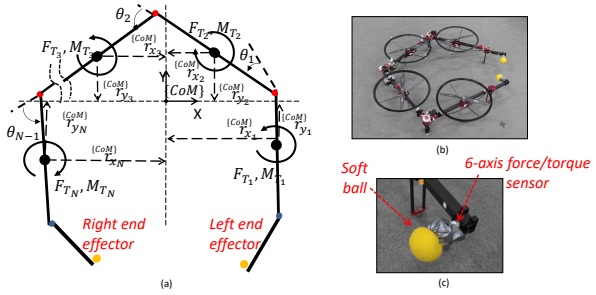

Fig. 2. HYDRUS robot with end effector. (a) shows the kinematic model, (b) shows the real robot is deployed with two grippers, and (c) shows the end effector equipped with 6-axis FT sensor and soft ball to increase friction.

III. Modeling and Contact Wrench Compensation

In our previous research [9], a Linear Quadratic Integral (LQI) controller is implemented to keep stability during maneuvering. In this paper, we extend LQI controller with compensation for contact wrench in end effectors.

A. System Model

We assume joints motion being slow during transformation, the robot could be approximated to be a single-rigid-body model at each time point. Considering the external wrench implemented on both end effectors, the translational and rotational equation would be modified as:

$$M^{\{W\}}\ddot{\boldsymbol{r}} = {}^{\{W\}}\boldsymbol{R}_{\{CoM\}} \begin{bmatrix} 0 \\ 0 \\ \sum_{i=1}^{4} F_{\mathrm{T}_i} \end{bmatrix} + {}^{\{W\}}\boldsymbol{f}_{\text{ext}} + \begin{bmatrix} 0 \\ 0 \\ -Mg \end{bmatrix} \tag{1}$$

$${}^{\{CoM\}}(I\dot{\boldsymbol{w}}) = \begin{bmatrix} \sum_{i=1}^{4} {}^{\{CoM\}}p_{\mathrm{y}_i} F_{\mathrm{T}_i} \\ -\sum_{i=1}^{4} {}^{\{CoM\}}p_{\mathrm{x}_i} F_{\mathrm{T}_i} \\ \sum_{i=1}^{4} c_i F_{\mathrm{T}_i} \end{bmatrix} + {}^{\{CoM\}}\boldsymbol{\tau}_{\text{ext}} - {}^{\{CoM\}}\boldsymbol{w} \times {}^{\{CoM\}}(I\boldsymbol{w}) \tag{2}$$

where $\{CoM\}$ and $\{W\}$ denote center of mass and world reference frame, $\ddot{\boldsymbol{r}} \in R^3$ denotes the linear acceleration of CoM, F_{T_i} denotes thrust force of i-th rotor, $\boldsymbol{f}_{\text{ext}} \in R^3$ and $\boldsymbol{\tau}_{\text{ext}} \in R^3$ denote the sum of external wrench in end effectors, p_{x_i} and p_{y_i} correspond to robot configuration and denote the distance between rotor and CoM, c_i denote drag moment coefficient of i-th rotor.

B. Contact Wrench Compensation

The compensated wrench are updated from force planner which would be introduced in Sec. V. The system architecture is as Fig. 3. Based on robot configuration, the compensated torque could be computed in the body frame and force in the world frame.

The previous work [9] utilizes integral term to compensate for contact wrench in object grasping. The main disadvantage is that the contact is not carefully modeled and robot would cause dangerous drift when grasping state changes.

Instead of from FT sensors directly, we update the compensated wrench from force planner and react with admittance controller. Since the unneglectable ground effect and downwash in aerial robots, contact force varies frequently in unexpected way. During grasping, robot is expected to be stable with less vibration, otherwise it is easy to break the contact between end effector and contact surface. Consequently, we develop an admittance controller along current position/attitude controller to react to the external force.

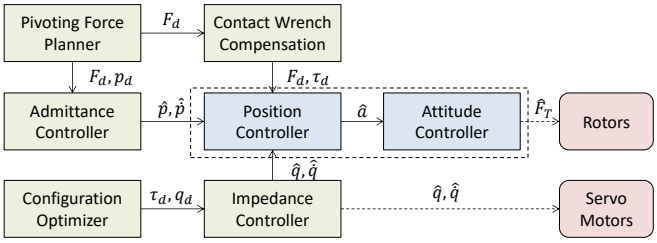

Fig. 3. The system architecture of whole framework. Position and attitude controller is developed in our previous work [9]. Contact wrench compensation is in Sec. III, configuration optimizer in Sec. IV, pivoting force planner in Sec. V, admittance and impedance controller in Sec. VI.

IV. Optimal Grasping Configuration

Since our HYDRUS robot could change its shape during the flight, there are a large number of potential grasping configuration as Fig. 4. The important problem is to optimize the optimal grasping configuration, considering not only rotor thrust limit, and also joints torque limit. In this section, the evaluation of stability in flight controller and joints torque effort in interaction task would be introduced to optimize grasping configuration.

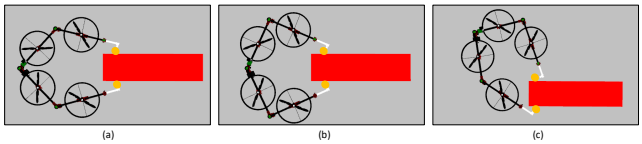

Fig. 4. Examples of potential grasping configuration. (a) and (b) are symmetrical in joint space, (c) is an asymmetrical example.

A. Thrust in Grasping Configuration

In HYDRUS robot, different configuration would vary obviously in thrust force distribution and maximum torque generation. Since the rotor thrust force could not exceed its upper bound, several of configuration is even infeasible.

In order to analyze the force distribution of each rotor, we assume the robot is in hovering state. Considering the translational and rotational equation in (1) and (2), the hovering state implies that all the linear and angular velocity/acceleration to be 0. In grasping task, two more constraints on configuration are robot end effectors in contact with object and configuration being symmetrical.

$$\boldsymbol{F}_{\mathrm{T}} = \boldsymbol{Q}^{-1} \begin{bmatrix} -\boldsymbol{\tau}_{\mathrm{ext}} \\ Mg - f_{\mathrm{ext}_z} \end{bmatrix} \tag{3}$$

$$subject\ to \quad \boldsymbol{Q} = \begin{bmatrix} p_{\mathrm{y}_1} & p_{\mathrm{y}_2} & p_{\mathrm{y}_3} & p_{\mathrm{y}_4} \\ -p_{\mathrm{x}_1} & -p_{\mathrm{x}_2} & -p_{\mathrm{x}_3} & -p_{\mathrm{x}_4} \\ c_1 & c_2 & c_3 & c_4 \\ 1 & 1 & 1 & 1 \end{bmatrix}$$

$$\boldsymbol{S}(p_{x_i}, p_{y_i}) = \mathbf{0}, \quad \boldsymbol{D}(p_{x_i}, p_{y_i}, object) = \mathbf{0}$$

where $\boldsymbol{F}_{\mathrm{T}} \in R^4$ denotes the thrust force of each rotor, p_{x_i} and p_{y_i} imply the joint configuration, $\boldsymbol{S}(p_{\mathrm{x}_i}, p_{\mathrm{y}_i}) = 0$ denotes the symmetry constraints, $\boldsymbol{D}(p_{\mathrm{x}_i}, p_{\mathrm{y}_i}, object) = 0$ denotes the contact constraints, and all the variables are in CoM reference frame.

Considering the downwash influence on object, the basic idea is to make it farthest counteract with itself under appropriate configuration. Since HYDRUS robot is in modular design with almost same weight and rotor in each link, the symmetrical configuration is the best strategy and the downwash perpendicular to symmetry axis could be farthest counteracted. The constraint is denoted as $\boldsymbol{S}(p_{\mathrm{x}_i}, p_{\mathrm{y}_i}) = 0$.

In contact constraints, $\boldsymbol{D}(p_{\mathrm{x}_i}, p_{\mathrm{y}_i}, object)$ calculates the distance between end effector and preset grasping point. The function value would be $\mathbf{0}$ while being in contact.

Based on the above two constraints, all the potential grasping configuration could be generated. Note that there are two kinds of infeasible configuration in our transformable aerial robot, including matrix $\boldsymbol{Q}$ not being invertible, or $\boldsymbol{Q}$ being invertible but the thrust force in saturation.

B. Flight Controller Stability in Interaction Task

For grasping task, we evaluate the aerial stability mainly in two components. One is the recovering ability when in external disturbance, the other is the maximum momentum could be generated when being commanded.

The first term could be approximated by variance value of the distributed rotor thrust force. The large variance value infers there is at least one rotor being close to its saturation state. External disturbance could easily make drone lose the controllability. On the contrary, the low variance value implies the robot has stronger ability to resist disturbance during the task.

The second term is also important in manipulation tasks and reflects the potentials in manipulation ability. It could be denoted by calculating the maximum residual momentum in three axes.

The optimization function for stability in flight controller would be:

$$\max_{\boldsymbol{q}} \left(-\lambda_{\mathrm{var}}\ var(\boldsymbol{F}_T(\boldsymbol{q})) + \lambda_{\mathrm{mt}}\ mt(\boldsymbol{q})\right) \tag{4}$$

$$subject\ to \quad constraints\ in\ (3),$$

$$\mathrm{Thrust}_{min} \leq F_{T_i} \leq \mathrm{Thrust}_{max}$$

$$\boldsymbol{q} \notin C_{\mathrm{self-collision}}$$

where $\boldsymbol{q} \in R^3$ denotes HYDRUS joints angle which refers to the configuration of robot, $var()$ denotes the variance function in statistics, $mt()$ denotes the function of maximum momentum generation declared above, $C_{\text{self}-\text{collision}}$ denotes the self-collided configuration which is infeasible for transformation. For example, if all the joints angle is large than $90°$, the rotor protector of HYDRUS robot would collide into each other and cause undesired damages.

C. Joints Effort in Interaction Task

In grasping task, another important item to consider is to keep joints effort in a reasonable range. For transformable aerial robot like HYDRUS robot, the design is the combination of manipulator arm and mutlirotor robot. The system could be approximated to be static in manipulation state since the translational and rotational motion of CoM is in slow speed. Joints effort could be analyzed separately under the framework of manipulator arm.

Consequently, we simplify the task into a two-dimensional grasping problem with the assumption of all the force in z axis being compensated by flight controller, and robot being flat with attitude in roll and pitch axis being 0. The force compensated by rotor thrust consists of gravity of robot and grasping force in z axis applied to the object. Therefore, the manipulation mechanics of HYDRUS robot with 3 joints could be described as:

$$\begin{bmatrix} \mathbf{0}_4 \\ \boldsymbol{\tau}_{\text{joints}} \end{bmatrix} + \boldsymbol{J}_{\text{Ef}_l}^{\text{T}} \boldsymbol{f}_{\text{Ef}_l} + \boldsymbol{J}_{\text{Ef}_r}^{\text{T}} \boldsymbol{f}_{\text{Ef}_r} = \mathbf{0}_{4+3} \tag{5}$$

where $\boldsymbol{\tau}_{\text{joints}} \in R^3$ denotes joints torque, $\boldsymbol{f}_{\text{Ef}_l} \in R^2$ and $\boldsymbol{f}_{\text{Ef}_r} \in R^2$ denote the contact force on left and right end effector, $\boldsymbol{J}_{\text{Ef}_l} \in R^{2\times 7}$ and $\boldsymbol{J}_{\text{Ef}_r} \in R^{2\times 7}$ denote the reduced Jacobian matrix of two end effector.

The contact force of two end effector could be the prior knowledge which is optimized by force planner in Sec. V based on the friction coefficients between effector and object. Therefore, in order to obtain the optimal grasping configuration, the joints effort should also be optimized as:

$$\begin{aligned} \min_{\boldsymbol{q}} \ & (\lambda_{sum}\ \boldsymbol{\tau}_{\text{joints}}^{\text{T}} \boldsymbol{\tau}_{\text{joints}} + \lambda_\tau\ var(\boldsymbol{\tau}_{\text{joints}})) \\ & \textit{subject to} \quad \textit{constraints in } (5), \\ & \tau_{\text{joints}_i} \leq \text{Torque}_{max} \\ & \boldsymbol{q} \notin C_{\text{self}-\text{collision}} \end{aligned} \tag{6}$$

where $var()$ denotes the variance function in statistics, $C_{\text{self}-\text{collision}}$ denotes the self-collided configuration as the previous definition.

D. Discussion

In the end, the above optimization target (4) and (6) would be put together into one function to obtain the optimal grasping configuration. Evidently, it is difficult to compute the analytical solution in this optimization problem since it is complex and highly non-linear. But in numerical way, the optimal results could be conveniently computed by discritizing robot configuration in joint space. These computation would be implemented offline and provide result as the prior knowledge to the following pivoting task.

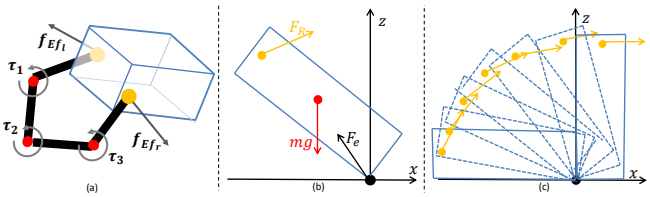

Fig. 5. The analysis of mechanics in grasping and pivoting task, and the concept of sequential force planner. (a) shows grasping analysis in Sec. IV, denoting the realtionship between joints effort and contact force from the end effectors. (b) shows the simplified 2D pivoting problem in Sec. V, including the grasping join force, object gravity and ground applied force. (c) shows the concept of sequential grasping force optimization in Sec. V-C.

V. Pivoting Force Planner

There are several approaches in re-orienting an long object as being perpendicular against the ground surface, such as lifting it to high place then utilizing gravity to naturally make it vertical, throwing and re-catching, or utilizing inertia force to swing the box like the inverted pendulum.

Considering the features of aerial robots being underactuated and lightweight with limited payload and agility, our pivoting strategy is to rotate the object along the edge of its base surface. It could make the best use of the contact force with ground to ease the rotor from being saturated. The robot only requires almost half of the strength by carefully optimized pivoting. It is especially efficient to deal with the heavy objects. Also low rotational friction benefits.

A. 2D Pivoting Problem

When grasping an object, the configuration of HYDRUS robot being symmetrical and end effectors in same contact force is the best strategy. As described above, the downwash influence applied on object could be less compared to a random configuration. Also, the same contact force from end effectors could balance the momentum and diminish the undesirable rotation in z axis.

Considering the join of ideally symmetrical grasping force, for the long box with respectively short width, our problem could be approximated as a 2-dimensional pivoting task as Fig. 5(b). There are only 2 contact force to analyze, namely the contact between box and ground, box and end effector, since the latter is symmetrically applied on the object.

B. Pivoting Mechanics

In this research, we adopt the quasi-static assumption [20] where the inertia force, Coriolis force and centrifugal force would not be included.

In most of the extrinsic pivoting tasks, the pivoting is in slow speed to not break the static friction. Consequently, the mechanics could be analyzed as an equilibrium model at each time point. In each equilibrium state, the force and momentum could be denoted as:

$$\boldsymbol{f}_{\text{R}} + \boldsymbol{f}_{\text{e}} - m\boldsymbol{g} = \mathbf{0} \tag{7}$$

$$\boldsymbol{p}_{\text{R}} \times \boldsymbol{f}_{\text{R}} + \boldsymbol{p}_{\text{e}} \times \boldsymbol{f}_{\text{e}} - \boldsymbol{p}_g \times m\boldsymbol{g} = \mathbf{0} \tag{8}$$

where $\boldsymbol{f}_{\mathrm{R}} \in R^2$ and $\boldsymbol{f}_{\mathrm{e}} \in R^2$ denote the total grasping force and ground applied force, $\boldsymbol{p}_{\mathrm{R}} \in R^2$, $\boldsymbol{p}_{\mathrm{e}} \in R^2$ and $\boldsymbol{p}_g \in R^2$ denote the moment arm of each force. Since the robot is assumed to stay in equilibrium state, the equation of force and torque are equal to zero on its right side.

We assume the contact between box and ground following Coulomb friction constraints. The contact force lies in friction cone as:

$$\boldsymbol{C}\boldsymbol{f}_{\mathrm{e}} \geq \boldsymbol{0} \tag{9}$$

$$\boldsymbol{C} = \begin{bmatrix} -1 & \mu \\ 1 & \mu \end{bmatrix} \tag{10}$$

where μ is the Coulomb friction coefficient.

C. Force Planner with Airflow Resistance

Different from pivoting tasks in manipulator arm or humanoid robot, there is one more challenge for aerial robot which is the airflow influence during the whole regrasping process [37].

Compared to ordinary airflow influence such as ground effect in quadrotor robots, pivoting task is more complex where the shape of grasped object would also affect the airflow. What is worse, the object would vary a lot in different manipulation tasks. Although there are several of recent work shows impressive performance with landing and taking off [29], [38], the airflow estimation during manipulation task is still an open question.

Considering the unquantifiable and unneglectable airflow effect, our strategy is to maximize friction force with respect to the different period to minimize its influence.

Therefore, to diminish the influence of airflow, robot underactuation and payload limitation, our optimization target including maximizing the friction residual term, minimizing the variation of grasping force between adjacent equilibrium state and minimizing total grasping force.

$$\begin{aligned} \min_{\boldsymbol{f}_{\mathrm{R}_i}} \; & (-\boldsymbol{V}_{\epsilon_i}\boldsymbol{\epsilon_i} + \boldsymbol{f}_{\mathrm{R}_i}^T \boldsymbol{W}_{\mathrm{R}_i} \boldsymbol{f}_{\mathrm{R}_i} + \delta \boldsymbol{f}_{\mathrm{R}_i}^T \boldsymbol{W}_{\delta_i} \delta \boldsymbol{f}_{\mathrm{R}_i}) \\ & \textit{subject to} \qquad \boldsymbol{C}\boldsymbol{f}_{\mathrm{e}_i} \geq \boldsymbol{\epsilon}_i, \quad \epsilon_i \geq \boldsymbol{0} \\ & \delta \boldsymbol{f}_{\mathrm{R}_i} = \boldsymbol{f}_{\mathrm{R}_i} - \boldsymbol{f}_{\mathrm{R}_{i-1}} \\ & \textit{equilibrium constraints in (7) and (8)} \end{aligned} \tag{11}$$

where a constrained quadratic programming (QP) problem is formed and could be solved with efficient algorithm [39].

We decompose the whole pivoting procedure into several states, depending on the rotation angle of box and ground. As concept in Fig. 5(c), the angle starts from 0° to 90° with fixed interval. The procedure is summarized in Alg.1.

Algorithm 1 Sequential Grasping Force Optimization (GFO)

```
procedure SEQUNTIAL GFO
    PrevOptForce ← 0
    for BoxRotationAngle ← 0° to 90° do
        OptForce ← SingleGFO( PrevOptForce, BoxRotationAngle)  ▷ SingleGFO() is function in (11)
        PrevOptForce ← OptForce
    end for
end procedure
```

VI. Interaction Controller

Based on the optimal grasping configuration and pivoting force planner, the target state in joint space and task space is optimized and to be integrated into robot controller.

In this section, we would introduce the impedance controller in joint space and admittance controller in task space to follow the target state. The implementation of two controller and further discussion about selection reasons would be introduced in next three subsection.

A. Impedance Controller in Joint Space

As the analysis in Sec. IV, given a grasping task, robot configuration is optimized with feasible joints effort. Given the target joint state, we build the impedance controller [40] in joint space to keep end effector in contact with object.

$$\boldsymbol{\tau}_d - \hat{\boldsymbol{\tau}} = \boldsymbol{K}_\tau(\boldsymbol{q}_{\mathrm{d}} - \hat{\boldsymbol{q}}) + \boldsymbol{D}_\tau(\dot{\boldsymbol{q}}_{\mathbf{d}} - \hat{\dot{\boldsymbol{q}}}) + \boldsymbol{M}_\tau(\ddot{\boldsymbol{q}}_{\mathbf{d}} - \hat{\ddot{\boldsymbol{q}}})$$

where $\boldsymbol{q} \in R^3$ denotes joints rotation angle, $\boldsymbol{\tau}_{\mathrm{d}} \in R^3$ and $\hat{\boldsymbol{\tau}} \in R^3$ denote the desired and measured joints of HYDRUS robot, $\boldsymbol{K}, \boldsymbol{D}, \boldsymbol{M} \in R^{3\times3}$, denote the stiffness, damping and inertia matrix of impedance controller. In our grasping task, $\dot{\boldsymbol{q}}_{\mathbf{d}}$ and $\ddot{\boldsymbol{q}}_{\mathbf{d}}$ keep $\mathbf{0}$ for stable contact.

B. Admittance Controller in Task Space

As force planner described in Sec. V, robot would receive discrete force and position command depending on its pivoting state. Since there are inevitable modeling errors and evident external disturbance, exactly precise force and position tracking is impossible. Inspired by [6], [7], [26], [29], [32], [41], we build an admittance controller for state tracking in the task space as follow:

$$-\boldsymbol{M}_{\mathrm{x}}\hat{\ddot{\boldsymbol{p}}} - \boldsymbol{D}_{\mathrm{x}}\hat{\dot{\boldsymbol{p}}} + \boldsymbol{K}_{\mathrm{x}}(\boldsymbol{p}_{\mathrm{d}}(t) - \hat{\boldsymbol{p}}) = \boldsymbol{f}_{\mathrm{d}}(t) - \hat{\boldsymbol{f}}$$

where $\boldsymbol{p}_{\mathrm{d}}(t)$ and $\boldsymbol{f}_{\mathrm{d}}(t)$ are obtained from the results of force planner in Sec. V-C, $\boldsymbol{K}_{\mathrm{x}}, \boldsymbol{D}_{\mathrm{x}}, \boldsymbol{M}_{\mathrm{x}}$ denote admittance spring, damping gain and inertia matrix.

Since our pivoting task is two-dimensional, the admittance controller reacts for the motion in x and z axis. Considering the steady state velocity introduced in [29] and combined structure of admittance controller and previous position controller, we pick $\boldsymbol{M}_{\mathrm{x}} = 0$ and generate reference position and velocity command to HYDRUS position controller as Fig. 3.

C. Discussion

We implement an impedance controller in joint space and admittance controller in task space for aerial pivoting task.

Compared to joint space, there are large modeling errors of contact and strong external disturbance caused by downwash in task space. The admittance controller being in passive fashion and controlling motion after force [41] is more beneficial for our task.

Another advantage for flight controller is admittance controller could be implemented outside of the existing position controller as Fig. 3 without large replacement. Since the position controller is the basic component for most of the multirotor robot, the whole framework could be easier to transfer between different platform.

VII. Experiment

In this chapter, we validate our framework by implementing the pivoting experiment with HYDRUS robot.

A. Flight Controller Compensation

We conduct the experiment by suddenly adding and removing contact under the flight controller with or without contact compensation. As shown in the attached video, when adding or removing contact, there is evident drift in controller without compensation. The drift is caused by the lagging of integral term in LQI controller when balancing the unmodeled term.

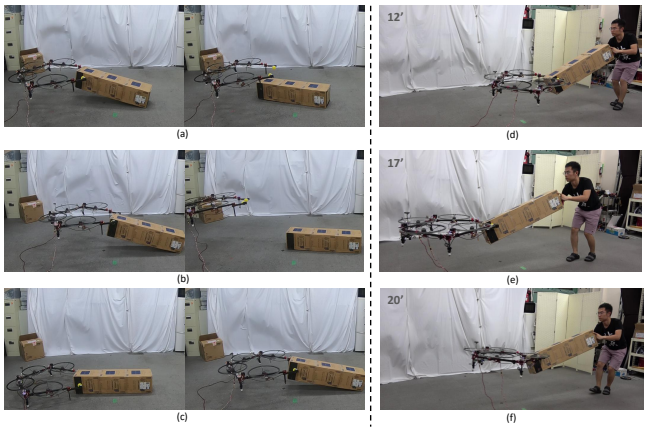

Fig. 6. Experiments of flight controller compensation and interaction control. (a) is flight controller with compensation when object is suddenly released. (b), (c) are flight controller without compensation, where there is evident drift in position. (d)-(f) are interaction control verification in cooperation task.

B. Interaction Controller

As shown in video, we validate the admittance controller in x axis with a cooperative transportation task. Different from pivoting task, we pick $\boldsymbol{K}_x = \mathbf{0}$ to guarantee human could move robot freely.

C. Pivoting Experiment

In pivoting task, we build a box with 1.08-m height and 0.26-m square base. The total mass is 1.06 kg, close to the payload upper bound (1.2 kg) of HYDRUS robot. We attach a soft ball on each end effector and paste antiskid tape on box to increase contact friction. This paper focuses on planner and controller so that perception is not integrated yet. The rotation angle of box is estimated based on robot position and box geometry.

The pivoting process is as Fig. 7. Admittance controller is switched after hovering. Compared to the open-loop pivoting during taking off, the admittance controller could quickly adjust the external force to be in reasonable range with the tracking keeps error no more than $2N$. The errors come from several uncertainties in this experiment, including the position offset of grasping point, downwash influence on the box. For example, in the end of pivoting, the box is vertical with largest windward surface as Fig. 7(4). Since our optimization target in force planner includes maximizing the friction force between object and ground, the error of tracking force could be tolerated to prevent the box from breaking contact.

We conduct several groups of pivoting experiments, and more details could be referred in attached video.

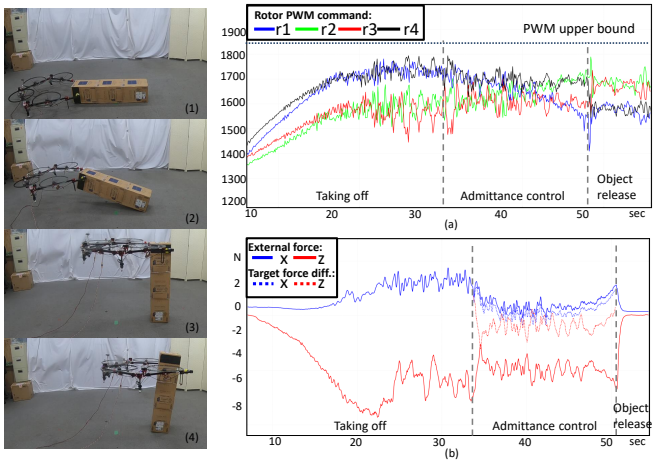

Fig. 7. Plots of pivoting experiment. There are 3 main steps inside the process, including robot taking off and hovering (1)-(2), admittance controller working to complete pivoting (2)-(3), and finally robot releasing object (3)-(4). (a) shows rotor PWM command (denoting the thrust force) during whole process, (b) shows the external force on end effectors and the deviation with target force from pivoting planner.

VIII. Conclusions and Future Work

In this paper, we introduce an aerial pivoting framework under the analysis of mechanics and constraints with extrinsic contact. The difference between aerial robot and humanoid or other manipulator is the former has aerodynamics influence such as downwash on the object and are highly underactuated with limited agility. The advantage is aerial robots have no constraint on the height, which enables them to pivot longer box compared to common manipulator arm or humanoid robot. Considering the limited payload ability of aerial robots, pivoting also enables them to manipulate the respectively heavy objects with the help of ground contact. In the end, we show the experiment of HYDRUS robot robustly pivoting a long box close to its payload upper bound.

For the future work, we will show the scalability of this framework with multiple robots to achieve cooperative regrasping, such as two robots pivoting the box in the air. Our final goal is to explore all the aerial manipulation skills to build motion primitives, and combine them to achieve aerial dexterous manipulation ability in architecture, rescue and even manufacturing scenarios.

Acknowledgments

The author would like to thank Weiwei Wan in Osaka Univ., Yifan Hou in Carnegie Mellon Univ., Kewei Xu in The Univ. of Miami, Yuanxin Shen in Georgia Tech, Zhonghui Zhu in Princeton Univ., Hironori Yoshida in The Univ. of Tokyo for their thoughtful discussions and suggestion.

REFERENCES

[1] Fabio Ruggiero, Vincenzo Lippiello, and Anibal Ollero. Aerial manipulation: A literature review. *IEEE Robotics and Automation Letters*, Vol. 3, No. 3, pp. 1957–1964, 2018.

[2] Justin Thomas, Joe Polin, Koushil Sreenath, and Vijay Kumar. Avian-inspired grasping for quadrotor micro uavs. In *ASME 2013 international design engineering technical conferences and computers and information in engineering conference*. American Society of Mechanical Engineers Digital Collection, 2014.

[3] Philipp Foehn, Davide Falanga, Naveen Kuppuswamy, Russ Tedrake, and Davide Scaramuzza. Fast trajectory optimization for agile quadrotor maneuvers with a cable-suspended payload. In *Robotics: Science and Systems*, pp. 1–10, 2017.

[4] E. Cataldi, F. Real, A. Suarez, P. A. Di Lillo, F. Pierri, G. Antonelli, F. Caccavale, G. Heredia, and A. Ollero. Set-based inverse kinematics control of an anthropomorphic dual arm aerial manipulator. In *2019 International Conference on Robotics and Automation (ICRA)*, pp. 2960–2966, May 2019.

[5] Nathan Michael, Jonathan Fink, and Vijay Kumar. Cooperative manipulation and transportation with aerial robots. *Autonomous Robots*, Vol. 30, No. 1, pp. 73–86, 2011.

[6] Andrea Tagliabue, Mina Kamel, Sebastian Verling, Roland Siegwart, and Juan Nieto. Collaborative transportation using mavs via passive force control. In *2017 IEEE International Conference on Robotics and Automation (ICRA)*, pp. 5766–5773. IEEE, 2017.

[7] Marco Tognon, Chiara Gabellieri, Lucia Pallottino, and Antonio Franchi. Aerial co-manipulation with cables: The role of internal force for equilibria, stability, and passivity. *IEEE Robotics and Automation Letters*, Vol. 3, No. 3, pp. 2577–2583, 2018.

[8] Moju Zhao, Tomoki Anzai, Fan Shi, Xiangyu Chen, Kei Okada, and Masayuki Inaba. Design, modeling, and control of an aerial robot dragon: A dual-rotor-embedded multilink robot with the ability of multi-degree-of-freedom aerial transformation. *IEEE Robotics and Automation Letters*, Vol. 3, No. 2, pp. 1176–1183, 2018.

[9] Moju Zhao, Koji Kawasaki, Tomoki Anzai, Xiangyu Chen, Shintaro Noda, Fan Shi, Kei Okada, and Masayuki Inaba. Transformable multirotor with two-dimensional multilinks: Modeling, control, and whole-body aerial manipulation. *The International Journal of Robotics Research*, Vol. 37, No. 9, pp. 1085–1112, 2018.

[10] B. Gabrich, D. Saldaa, V. Kumar, and M. Yim. A flying gripper based on cuboid modular robots. In *2018 IEEE International Conference on Robotics and Automation (ICRA)*, pp. 7024–7030, May 2018.

[11] Davide Falanga, Kevin Kleber, Stefano Mintchev, Dario Floreano, and Davide Scaramuzza. The foldable drone: A morphing quadrotor that can squeeze and fly. *IEEE Robot. Autom. Lett.*, Vol. 4, No. 2, pp. 209–216, April 2019.

[12] Hyunsoo Yang, Sangyul Park, Jeongseob Lee, Joonmo Ahn, Dongwon Son, and Dongjun Lee. Lasdra: Large-size aerial skeleton system with distributed rotor actuation. In *2018 IEEE International Conference on Robotics and Automation (ICRA)*, pp. 7017–7023. IEEE, 2018.

[13] Marko Car, Antun Ivanovic, Matko Orsag, and Stjepan Bogdan. Impedance based force control for aerial robot peg-in-hole insertion tasks. In *2018 IEEE/RSJ International Conference on Intelligent Robots and Systems (IROS)*, pp. 6734–6739. IEEE, 2018.

[14] Sangyul Park, Jeongseob Lee, Joonmo Ahn, Myungsin Kim, Jongbeom Her, Gi-Hun Yang, and Dongjun Lee. Odar: Aerial manipulation platform enabling omnidirectional wrench generation. *IEEE/ASME Transactions on mechatronics*, Vol. 23, No. 4, pp. 1907–1918, 2018.

[15] Markus Ryll, Giuseppe Muscio, Francesco Pierri, Elisabetta Cataldi, Gianluca Antonelli, Fabrizio Caccavale, Davide Bicego, and Antonio Franchi. 6d interaction control with aerial robots: The flying end-effector paradigm. *The International Journal of Robotics Research*, Vol. 38, No. 9, pp. 1045–1062, 2019.

[16] J Kenneth Salisbury and B Roth. Kinematic and force analysis of articulated mechanical hands. *Journal of Mechanisms, Transmissions, and Automation in Design*, Vol. 105, No. 1, pp. 35–41, 1983.

[17] Yasumichi Aiyama, Masayuki Inaba, and Hirochika Inoue. Pivoting: A new method of graspless manipulation of object by robot fingers. In *Proceedings of 1993 IEEE/RSJ International Conference on Intelligent Robots and Systems (IROS'93)*, Vol. 1, pp. 136–143. IEEE, 1993.

[18] Antonio Bicchi. Hands for dexterous manipulation and robust grasping: A difficult road toward simplicity. *IEEE Transactions on robotics and automation*, Vol. 16, No. 6, pp. 652–662, 2000.

[19] Pierre Tournassoud, Tomás Lozano-Pérez, and Emmanuel Mazer. Regrasping. In *Proceedings. 1987 IEEE International Conference on Robotics and Automation*, Vol. 4, pp. 1924–1928. IEEE, 1987.

[20] Nikhil Chavan Dafle, Alberto Rodriguez, Robert Paolini, Bowei Tang, Siddhartha S Srinivasa, Michael Erdmann, Matthew T Mason, Ivan Lundberg, Harald Staab, and Thomas Fuhlbrigge. Extrinsic dexterity: In-hand manipulation with external forces. In *2014 IEEE International Conference on Robotics and Automation (ICRA)*, pp. 1578–1585. IEEE, 2014.

[21] Weiwei Wan and Kensuke Harada. Developing and comparing single-arm and dual-arm regrasp. *IEEE Robotics and Automation Letters*, Vol. 1, No. 1, pp. 243–250, 2016.

[22] Yifan Hou and Matthew T Mason. Robust execution of contact-rich motion plans by hybrid force-velocity control. *arXiv preprint arXiv:1903.02715*, 2019.

[23] Eiichi Yoshida, Mathieu Poirier, Jean-Paul Laumond, Oussama Kanoun, Florent Lamiraux, Rachid Alami, and Kazuhito Yokoi. Regrasp planning for pivoting manipulation by a humanoid robot. In *2009 IEEE International Conference on Robotics and Automation*, pp. 2467–2472. IEEE, 2009.

[24] Masaki Murooka, Shintaro Noda, Shunichi Nozawa, Yohei Kakiuchi, Kei Okada, and Masayuki Inaba. Manipulation strategy decision and execution based on strategy proving operation for carrying large and heavy objects. In *2014 IEEE International Conference on Robotics and Automation (ICRA)*, pp. 3425–3432. IEEE, 2014.

[25] Fan Shi, Moju Zhao, Weiwei Wan, Kei Okada, and Masayuki Inaba. Aerial regrasping: Exploring active dynamic regrasps with transformable multilink drone. In *ICRA 2019 Workshop on Toward Online Optimal Control of Dynamic Robots*. Citeseer, 2019.

[26] Nicolas Staub, Davide Bicego, Quentin Sablé, Victor Arellano, Subodh Mishra, and Antonio Franchi. Towards a flying assistant paradigm: The othex. In *2018 IEEE International Conference on Robotics and Automation (ICRA)*, pp. 6997–7002. IEEE, 2018.

[27] Fan Shi, Moju Zhao, Tomoki Anzai, Keita Ito, Xiangyu Chen, Shunichi Nozawa, Kei Okada, and Masayuki Inaba. Multi-rigid-body dynamics and online model predictive control for transformable multi-links aerial robot. *Advanced Robotics*, pp. 1–14, 2019.

[28] Steven Bellens, Joris De Schutter, and Herman Bruyninckx. A hybrid pose/wrench control framework for quadrotor helicopters. In *Robotics and Automation (ICRA), 2012 IEEE International Conference on*, pp. 2269–2274. IEEE, 2012.

[29] Teodor Tomić, Christian Ott, and Sami Haddadin. External wrench estimation, collision detection, and reflex reaction for flying robots. *IEEE Transactions on Robotics*, Vol. 33, No. 6, pp. 1467–1482, 2017.

[30] Kostas Alexis, Georgios Darivianakis, Michael Burri, and Roland Siegwart. Aerial robotic contact-based inspection: planning and control. *Autonomous Robots*, Vol. 40, No. 4, pp. 631–655, 2016.

[31] Fan Shi, Moju Zhao, Tomoki Anzai, Xiangyu Chen, Kei Okada, and Masayuki Inaba. External wrench estimation for multilink aerial robot by center of mass estimator based on distributed imu system. In *2019 IEEE International Conference on Robotics and Automation (ICRA)*, May 2019.

[32] Federico Augugliaro and Raffaello D'Andrea. Admittance control for physical human-quadrocopter interaction. In *Control Conference (ECC), 2013 European*, pp. 1805–1810. IEEE, 2013.

[33] F. Forte, R. Naldi, A. Macchelli, and L. Marconi. Impedance control of an aerial manipulator. In *2012 American Control Conference (ACC)*, pp. 3839–3844, June 2012.

[34] Vincenzo Lippiello and Fabio Ruggiero. Cartesian impedance control of a uav with a robotic arm. *IFAC Proceedings Volumes*, Vol. 45, No. 22, pp. 704–709, 2012.

[35] Yiannis Karayiannidis, Christian Smith, Danica Kragic, et al. Adaptive control for pivoting with visual and tactile feedback. In *2016 IEEE International Conference on Robotics and Automation (ICRA)*, pp. 399–406. IEEE, 2016.

[36] Yifan Hou, Zhenzhong Jia, Aaron M Johnson, and Matthew T Mason. Robust planar dynamic pivoting by regulating inertial and grip forces. In *Workshop Algorithmic Found. Robot., 12th, San Francisco, Dec*, Vol. 18, p. 20, 2016.

[37] Derrick Yeo, Elena Shrestha, Derek A Paley, and Ella M Atkins. An empirical model of rotorcrafy uav downwash for disturbance localization and avoidance. In *AIAA Atmospheric Flight Mechanics Conference*, p. 1685, 2015.

[38] Guanya Shi, Xichen Shi, Michael O'Connell, Rose Yu, Kamyar Azizzadenesheli, Animashree Anandkumar, Yisong Yue, and Soon-

Jo Chung. Neural lander: Stable drone landing control using learned dynamics. In *2019 International Conference on Robotics and Automation (ICRA)*, pp. 9784–9790. IEEE, 2019.

[39] H.J. Ferreau, C. Kirches, A. Potschka, H.G. Bock, and M. Diehl. qpOASES: A parametric active-set algorithm for quadratic programming. *Mathematical Programming Computation*, Vol. 6, No. 4, pp. 327–363, 2014.

[40] Neville Hogan. Impedance control: An approach to manipulation: Part i-theory. *Journal of dynamic systems, measurement, and control*, Vol. 107, No. 1, pp. 1–7, 1985.

[41] Arvid QL Keemink, Herman van der Kooij, and Arno HA Stienen. Admittance control for physical human-robot interaction. *The International Journal of Robotics Research*, Vol. 37, No. 11, pp. 1421–1444, 2018.